Coherent directed movement toward food modeled in *Trichoplax*, a ciliated animal lacking a nervous system

Carolyn L. Smith[a,1,2], Thomas S. Reese[a,1,2], Tzipe Govezensky[b,1], and Rafael A. Barrio[c,1]

[a]National Institute of Neurological Disorders and Stroke, National Institutes of Health, Bethesda, MD 20892; [b]Instituto de Investigaciones Biomédicas, Universidad Nacional Autónoma de México, 04510 Mexico City, Mexico; and [c]Instituto de Física, Universidad Nacional Autónoma de México, 01000 Mexico City, Mexico

Contributed by Thomas S. Reese, March 1, 2019 (sent for review September 11, 2018; reviewed by Edwin Munro and Kevin J. Painter)

Trichoplax adhaerens **is a small, ciliated marine animal that glides on surfaces grazing upon algae, which it digests externally. It has no muscles or nervous system and only six cell types, all but two of which are embedded in its epithelium. The epithelial cells are joined by apical adherens junctions; neither tight junctions nor gap junctions are present. Monociliated epithelial cells on the lower surface propel gliding. The cilia beat regularly, but asynchronously, and transiently contact the substrate with each stroke. The animal moves in random directions in the absence of food. We show here that it exhibits chemotaxis, moving preferentially toward algae embedded in a disk of agar. We present a mathematical model to explain how coherent, directional movements could arise from the collective actions of a set of ciliated epithelial cells, each independently sensing and responding to a chemoattractant gradient. The model incorporates realistic values for viscoelastic properties of cells and produces coordinated movements and changes in body shape that resemble the actual movements of the animal. The model demonstrates that an animal can move coherently in search of food without any need for chemical signaling between cells and introduces a different approach to modeling behavior in primitive multicellular organisms.**

Placozoa | eukaryotic chemotaxis | coherent motion | multicellularity | directed migration

The small, ciliated animal *Trichoplax adhaerens* locomotes to hunt for food despite lacking muscles or a nervous system. It is a member of the phylum Placozoa, the taxon that many consider to be sister to the Eumetazoa (Cnidaria plus Bilateria). Porifera and Ctenophora are thought have diverged earlier (1–5). *Trichoplax* is roughly disk-shaped in outline, up to several millimeters in diameter but only ∼20 μm thick. Like all animals (6), it is bounded by an epithelium comprised of cells joined by junctions that fix the positions of the cells relative to one another (7). *Trichoplax* has no axis of symmetry and only six identified cell types, all but two of which are part of the epithelium (see ref. 8 and Fig. 1).

Trichoplax glides over surfaces, propelled by monociliated cells that account for a large proportion of the epithelial cells on its ventral surface (Fig. 1).

Since *Trichoplax* can glide in any direction, we infer that the axonemes of its cilia, which dictate the direction of beating (9–12), are not aligned in any particular direction and could have variable orientations. The ciliated epithelial cells of Ctenophores, Cnidaria, and Bilateria are electrically coupled by gap junctions composed of innexins or connexins (1, 13, 14), but no gap junctions have been found in *Trichoplax* by electron microscopy and no connexins or innexins have been identified in its genome (15).

Trichoplax also undergoes amoeboid-like changes in shape, movements that some have attributed to elongated fiber cells (16) residing in a space between the dorsal and ventral epithelia (Fig. 1). Whether or not fiber cells are contractile, they can provide an elastic scaffold holding bolding cells together. A recent report (17) demonstrates that cells of the dorsal epithelium are contractile and behave as a dynamic elastic sheet.

Trichoplax can be maintained in the laboratory on a diet of microalgae. Upon being placed in a dish containing algae, they pause to feed in areas where algae are abundant (18). Pausing is accompanied by arrest of ciliary beating, which is initiated by peptides secreted from a type of cell in the epithelium (Fig. 1) (18, 19). Each gland cell bears a cilium (19) that could be chemosensory and used to detect algae. Once a pause is initiated, the animal remains in place for several minutes while it feeds on the algae lying underneath the lower surface. Algae are digested by secretions from a second type of secretory cell, the lipophil (18), which is interspersed among the ciliated cells (ref. 18 and Fig. 1). Material released from the lysed algae is endocytosed by the overlying epithelial cells (7, 20). Movie S1 illustrates this behavior.

Many organisms, ranging in complexity from bacteria, protists, and fungi to metazoa, rely on chemotaxis to find food (21), and *Trichoplax* was reported to move toward glycine (22). The present work was motivated by our discovery that *Trichoplax* placed on a bed of agar containing a small clump of algae preferentially move toward the algae and remain near them despite being blocked from feeding upon them.

This behavior raises the question of how an array of cells possessing cilia that are able to beat in random directions produces a coherent movement of the whole animal and directs it to food?

Significance

Trichoplax **is a disk-shaped marine animal whose body plan and lifestyle could be similar to those of the Precambrian ancestor of many animals on earth today. It has only six cell types and no nervous system. It glides on substrates feeding on microalgae, propelled by asynchronously beating cilia. It can move in any direction, so we assume that its cilia do not have a uniform polarity and may be randomly oriented, unlike cilia in most epithelia. We show that *Trichoplax* exhibits chemotaxis and present a mathematical model to explain how directional movement could arise from collective actions of randomly oriented ciliated cells, each independently responding to a chemoattractant gradient but constrained by their attachments to other cells in the animal.**

Author contributions: C.L.S. and R.A.B. designed research; C.L.S. and R.A.B. performed research; R.A.B. contributed new reagents/analytic tools; C.L.S., T.S.R., T.G., and R.A.B. analyzed data; and C.L.S., T.S.R., and R.A.B. wrote the paper.

Reviewers: E.M., The University of Chicago; and K.J.P., Heriot-Watt University.

The authors declare no conflict of interest.

[1]C.L.S., T.S.R., T.G., and R.A.B contributed equally to this work.

[2]To whom correspondence may be addressed. Email: smithca@ninds.nih.gov or treese@mbl.edu.

This article contains supporting information online at www.pnas.org/lookup/suppl/doi:10.1073/pnas.1815655116/-/DCSupplemental.

Published online April 12, 2019.

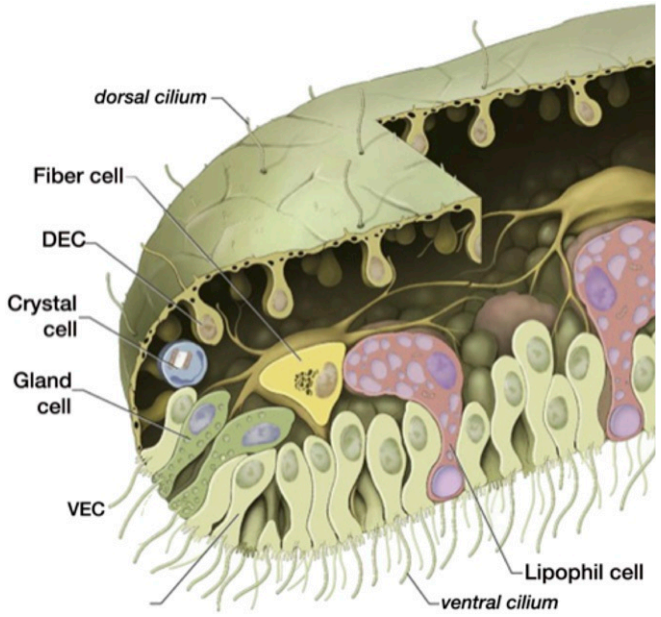

Fig. 1. Major cell types in *Trichoplax*. Facing the substrate (below) is a thick ventral plate composed of epithelial cells (VEC) (light green), each bearing a cilium and multiple microvilli; lipophil cells (brick) packed with large secretory granules containing digestive enzymes; and gland cells (green), distinguished by their contents of small secretory granules and prevalence near the rim. Dorsal epithelial cells (DEC) (tan) form a roof across the top of the animal. Fiber cells lying between the dorsal and ventral epithelia have long branching processes that contact the other cell types. A crystal cell (pale blue) containing a birefringent crystal lies under the dorsal epithelium near the rim. Reproduced from ref. 8. Copyright (2014), with permission from Elsevier.

There has been an increased interest in studying collective motion arising from random self-driven particles since the seminal work of Vicsek et al. (23), which modeled swarms of living individuals and tissues. This model is appropriate for swimming particles that align their velocities by hydrodynamic interactions (24). There are also models that do not impose alignment explicitly, collective motion arising from either inelastic collisions (25), short range radial forces (26), or active elastic membrane spring-like interactions (27). In these models, collective coherent motion appears as a first-order phase transition with the amount of disorder, or a jamming phase transition with increased density (28). The numerous models of locomotion developed for swimming ciliated protists and metazoans (see ref. 29) proved to be inadequate to explain locomotion of *Trichoplax*, since this animal does not swim but crawls. These models evoke hydrodynamic interactions between cilia to explain the metachronous beating of the cilia. Trichoplax cilia beat asynchronously and generate propulsion by pulling on the substrate. Hydrodynamic interactions are unlikely to come into play. Here, we take appropriate elements of these models to build a model that provides a simple physical explanation of directional chemotactic gliding in *Trichoplax*, based only on the known properties of its cellular components.

Results

***Trichoplax* Chemotax Toward Algae.** We looked for evidence of chemotactic behavior by observing the movements of animals placed on the surface of a bed of agar overlaying a small (3-mm) clump of algae (Movie S2). Animals that were placed >5 mm from the center of the clump of algae moved in random directions with respect to the algae. However, animals that were placed or wandered closer to the algae moved preferentially toward it. Thirty-seven out of 40 animals that came within 5 mm of the algae centroid eventually migrated over the algae. Upon reaching the algae, the animals typically remained nearby for the duration of the experiment. Only 1 of the 37 animals that migrated over the algae later moved >5 mm away.

Representative trajectories for six of nine animals that were tracked as they migrated onto the algae are illustrated in Fig. 2*A*. A change in the behavior of the animals as they came into the vicinity of the algae is apparent. The trajectories are meandering and frequently change directions while the animals are distant from the algae (pink, blue, red, and aqua tracks). When the centroids of the animals move within 5 mm of the algae, segments of the tracks that are directed toward the clump of algae are longer than segments directed elsewhere. Only one animal (green) that approached within 3 mm of the algae centroid subsequently moved >5 mm away. This animal later reversed direction to reach the algae. Plots of the distances between the centroids of animals and the algae over time show that four of the six animals (pink, blue, read, and teal) move faster and more persistently toward the algae than in other directions Fig. 2*B*. The meandering trajectories of the animals as they approach the algae are characteristic of a type of chemotaxis sometimes referred to as stochastic chemotaxis or "chemokinesis," to differentiate it from another type of chemotaxis in which the organism moves directly toward the attractant (21, 30, 31).

The preferential movement of the animals toward the algae suggests that the algae emit a chemical that attracts the animals. The algae were alive, so we can assume that they continuously emit the attractant. We expect that the concentration drops off steeply with distance because diffusion in agar is rapid ($D = (8.8 \pm 1.2) \times 10^{-6}$ cm^2/s), as obtained by measuring diffusion of a fluorescent dye in 1.7% agar.

Model of Coherent Motion Originated by Random Propulsions. Our aim is to build a model that is able to explain the emergence of coherent motion from random propulsions without having a regulatory system that choreographs the motion of thousands of individual cells. This coherent behavior should emerge from simple physical and chemical interactions among cells. We assume that the physical interactions can be described as forces acting on each individual cell. Therefore, the basic Newtonian equations of motion that each ciliated cell i obeys are

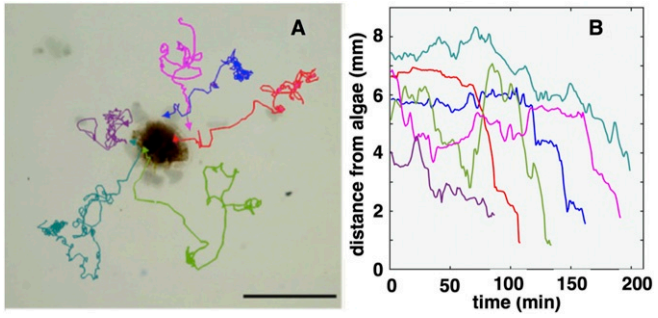

Fig. 2. Movements of *Trichoplax* in the presence of a focal food source. (*A*) Snapshot from Movie S2 showing positions of the animals after 8 h, when most of them had congregated near the algae. Colored tracks represent the trajectories of six animals. The segments of the trajectories represent distances moved by the centroid of the animal over 2-min intervals. (*B*) Distances of centroids of animals to algae for the six tracks illustrated in *A* versus the time spent reacting to the chemoattractant. Data points were measured at 10-s intervals.

$$m_i \frac{d\vec{v}(i,t)}{dt} = \vec{F}_t(i,t), \quad \textbf{[1a]}$$

$$\frac{d\vec{r}(i,t)}{dt} = \vec{v}(i,t), \quad \textbf{[1b]}$$

where $\vec{r}(i,t)$ and $\vec{v}(i,t)$ are the instantaneous position and velocity of cell i, and $\vec{F}_t(i)$ is the total force acting on each cell. Since we assume that all cells have the same mass ($m_i = m$), we consider $m = 1$ without loss of generality.

The most obvious force is the propulsion originated by the cilia. Microscopic observations indicate that the cilia beat regularly but asynchronously, transiently contacting the substrate during each beat (18). Our model assumes that each ciliated cell beats in an arbitrary direction and that the driving force comes exclusively from the movement of its cilium, which, when adhering to the surface and beating, produces a small displacement r_0 of the cell. If the cells were not connected to their neighbors, the individual motion of the cells would be a random walk, and the collection of cells would diffuse, with a quadratic mean displacement increasing linearly with time. The contribution of the ciliary strokes to the dynamics of each cell is labeled $\vec{v}_1$ (*SI Appendix*, section A.1).

However, the ciliated cells also are subject to forces arising from both direct and indirect connections to other cells in the animal. We consider the effects of these forces through their influence on the shapes and motions of the ciliated cells, which are situated in a plane. This allows us to build a model in two dimensions for the ventral ciliated cells. Furthermore, we assume that each ciliated cell is able to sense a chemoattractant emanating from the food source that biases its movement in the direction of the food.

In some cases, the force could be derived from a scalar field $\vec{F}_t(i) = -\nabla V(i)$. For example, the fact that the ventral cells are joined together imposes an elastic potential that tends to restore changes in size and shape of the cells due to the motion of neighbor cells. The easiest way to describe this elastic field would be to attach springs among pairs of points defining the cilia. This would be exactly the model used in ref. 27, which is able to produce steady translations of the sheet of masses with springs.

However, in our case, we are dealing with cells that have a given size and shape that should be restored during the collective motion. Therefore, we define an "elastic" potential, which is quadratic in the coordinates, containing two terms. The first one restores the volume (area in 2D) of the cells to an equilibrium value A_0. The second one restores the shape of the cells to be as isotropic (spherical or circular in 2D) as possible, by assuming that in equilibrium, the position of the center of mass of the cell should coincide with the position of the point that defines the cilium.

To do this, we define a Voronoi tessellation (*SI Appendix*, section A.2) in which we impose the abovementioned elastic field, with an additional friction term to account for dissipation (33, 34). It is seen that this force alone is able to produce a circular system of isotropic cells of the same size, starting with a random collection of points inscribed in a circle (*SI Appendix*, Fig. S2). This field simulates the fluid interactions among the ventral cells of the animal. It is clear that this field is acting continuously, not only when there is a ciliary stroke, and changes the value of the main dynamical quantity, which is the total velocity of the cell $\vec{v}(i,t)$. This field prevents the increase of volume due to diffusion, holding the random walkers together. However, the center of mass of the system would follow the trajectory of a random walker, so the whole animal visits an area that increases linearly in time.

There are additional elastic interactions coming from cells other than the neighbors. We observe that the dorsal epithelium is a plane connected to the ventral epithelium around the edge of the animal, but the rest of the dorsal epithelium has no connections with other cells in the animal except for some fiber cell processes. It has been shown (17) that cells of the dorsal epithelium are contractile but that their contractile movements occur independently of cells in the ventral epithelium. Due to the elasticity and contractility of the dorsal epithelial cells, the dorsal epithelium can exert a restoring force around the edge of the animal where it connects to the ventral epithelium. Therefore, we define an elastic field acting on the peripheral cells that restores the distance of these cells from the center of mass of the animal to a given value congruent to the radius of the animal in equilibrium (*SI Appendix*, section A.3). The contribution to the dynamics of the cell due to this interaction is called $\vec{v}_2(i,t)$. This depends on three parameters, namely the spring constant k_p, the equilibrium radius of the animal R, and the damping coefficient κ_p.

Finally, another medium range interaction is present due to the fiber cells, which connect distant ventral (and dorsal) cells. The elastic interactions that we have already considered produce the effect that each cell tries to copy the average velocity of its neighbors. The motion of swarms of birds or fish can be simulated by imposing this simple rule only. The effect of the fiber cell connections is being modeled by extending this rule by averaging the velocities of the cells within a certain radius d from the center of mass of each cell (*SI Appendix*, section A.4). This is the so-called Vicsek model, whose effect is to produce a coherent motion of cells in a region of a given size. The contribution to the dynamics of the cells of this interaction is called $\vec{v}_3(i.t)$. This adds another parameter to the model, namely, the relative strength of this interaction k_s.

Although chemotaxis is a widespread phenomenon in eukaryotic cells and bacteria, very little is known about chemotaxis in a group of attached cells. In view of this, we model chemotaxis in the simplest possible way, taking advantage of the fact that during the time the animal is moving around the food that emits the chemoattractant, the concentration profile of this substance does not change appreciably and can be considered fixed. As a result, there is a component of the velocity of each cell in the direction of the gradient of chemoattractant. Let us call this component $\vec{v}_4(i,t)$. The strength of this term is proportional to the chemotaxis sensitivity χ, and it is called A_f (*SI Appendix*, section B).

A detailed description of the model is given in *SI Appendix*.

Simulation. The total time-dependent velocity, which is the main dynamical function in Eq. **1b**, can thus be written as

$$\vec{v}(i,t) = \vec{v}_1(i,t) + \vec{v}_2(i,t) + \vec{v}_3(i,t) + \vec{v}_4(i,t), \quad \textbf{[2]}$$

where $\vec{v}_1$ represents the random motion of the cilium, the dorsal epithelial cells act as an elastic membrane and produce $\vec{v}_2$ acting on the edge of the animal, and $\vec{v}_3$ arises from the medium-range elastic interactions due to the fiber cells. Finally, $\vec{v}_4$ represent the effect of chemotaxis.

The equations of motion could be integrated numerically by discretizing the time, that is,

$$\vec{v}(i,t+\delta t) = \vec{v}(i,t) + \vec{F}(i,t)\delta t, \quad \textbf{[3]}$$

$$\vec{r}(i,t+\delta t) = \vec{r}(i,t) + \vec{v}(i,t)\delta t, \quad \textbf{[4]}$$

where a value between 0.01 and 0.05 for δt was used in all computer simulations. The unit of time is chosen so that the speed of the simulated animal matches the experimental observations, so it is possible to determine that $\delta t = 26$ s.

To mimic the locomotor and feeding behavior of the animal, our model must include a mechanism to stop ciliary beating when the animal reaches the food and to resume beating after the food

is consumed. Arrest of ciliary beating is thought to be elicited by a peptide secreted from gland cells upon detection of algae (19). For simplicity, our model excludes the gland cells and considers only the ciliated cells, which we postulate cease beating autonomously at a specific distance from food.

The gland cells of the animal are symmetrically situated around the center of mass. Therefore, at each time step, we test the distance between the center of mass and any food source, and if this distance is sufficiently small (we choose R/4), we stop the motion of the cilium and diminish gradually the amplitude of the food source until it is consumed. Then, we resume the normal motion.

With these ingredients at hand, we integrate the equations of motion and are able to mimic the chemotactic movements of animals toward algae. We show an example calculation in Movie S3. The parameters used for the simulation are depicted in Table 1. Compare Movie S3 to Movie S1, which shows a single Trichoplax gliding and feeding on algae.

The values shown in Table 1 are in arbitrary computer units. Several experimental movies (see, for example, Movies S1 and S2) were used to investigate the correspondence of computer units of distance and velocity to the ones measured experimentally. A computer unit distance corresponds to 25 μm, and a time unit is 26 s. The elastic module of the cell membrane was estimated to be of the order of 10 MPa (32, 35), which corresponds to 80 computer units for the elastic constants.

In Fig. 3*A*, we show the results from theoretical simulations of the motion of the animal in the presence of a single food source. In Fig. 3*B*, we plot the distance from the centroid of the animal to the food source. Note that chemotaxis is not directing the animal straight to the food source; there are hesitations and turns, just as in real animals (compare with Fig. 2; also see Movies S1 and S2). The continual changes in the relative positions of the cilia suggests the flow of a liquid material, similar to the flowing motions of particles in the interior of the real animal (Movie S1). The model also recapitulates to some extent the deformations of the outline of the animal while moving, although the magnitude of the deformations are larger in the real animal, where contractile cells may participate in changing its shape.

The very interesting sharp transition in Fig. 3*B* from random motion to a direct approach to the food, as observed in real animals, is a feature that arises from the competition between the strength of the chemotactic term and the random propulsion of the cilia. When far from the source, the concentration of chemoattractant is small and the random motion dominates. However, a nonzero v_4 slowly directs the cells toward regions with increasing concentration until a point is reached at which the chemotaxis dominates over the random propulsion. The behavior predicted by the model is complicated because the model is nonlinear and the action of very different phenomena that contribute to the final motion.

The sensitivity analysis performed in *SI Appendix*, section C showed that the system is robust against changing parameter values in a wide range (in the sense that the model produces qualitatively the same behavior). Once the elastic and geometrical parameters have been adjusted to mimic the real animal, the behavior changes when varying the Vicsek radius and the chemotactic sensitivity.

Table 1. Values of the parameters

Class	Variable name	Value
Animal parameters	Radius R	10
	Number of cells N	1,000
	Cell area A_0	0.7528
Elastic constants		
Dorsal membrane	Bulk modulus k_p	50
	Friction coefficient κ_p	10
Cell relaxation	Area restoring k_a	50
	Centroid restoring k_c	50
	Friction coefficient κ	10
Fiber cells	Strength k_s	67.6
	Viscek radius d	$15 \times d_{min}$
Domain		
$L \times L$	L	$8R$
Food landscape	Number of Gaussians n	1
	Amplitude A_m	2+0.8(ζ −0.5)
	Width σ_m	$4R + R\zeta(1, n)$
Feeding parameter	Food strength A_f	1.5

All are kept fixed in the simulations, except d and A_f.

Experimental Validation of the Model

Our model predicts that the animal moves toward the food in meandering trajectories that approach the source in a similar way as the observed animals. To quantify this similitude, we have examined the data to produce scatter plots of the dependence of the component of the velocity along the vector $\vec{R}_{cf}(t)$ that links the center of mass of the animal to the position of the food, as a function of the distance from the food source. Notice that $\vec{R}_{cf}(t)$ changes with time; thus, the velocity component in the direction of the food is $v_L = \frac{\vec{R}_{cf}(t)\cdot\vec{S}(t)}{|R_{cf}(t)|}$, where $\vec{S}(t) = \vec{r}_{cm}(t + \Delta t) - \vec{r}_{cm}(t)$. We examined eight different experimental measurements and eight randomly selected theoretical simulations. In both kinds of data, one notices that, on average, the velocity component in the direction of the food is larger than in the opposite direction, and, in general, it increases when approaching the food source.

In Fig. 4 we compare the experimental measurements (red) with the theoretical results (blue). The data have been smoothed to produce clearer scatter plots.

In Fig. 4*A*, we show the results when the animals are around the food source (between 1 and ∼9 mm). Notice that the animals show acceleration when approaching the food source and a sudden deceleration when they are very near. In Fig. 4*B*, we show the same scatter plot for animals far from the food source (between 6 and 18 mm). Notice that the behavior of both sets of data is very similar, partially validating the model.

The calculations in *SI Appendix*, section C demonstrate the importance of medium-range forces in the model. The elastic constants of the model should also be important. In *SI Appendix*, Fig. S4*B*, we show two ways of changing shape of the animal: (*i*) as the elastic constants (or the Viscek strength k_s) increase, the shape becomes less circular; and (*ii*) as the Viscek radius increases, the shape index becomes larger (more circular shape). The combined result of these dependencies is that when the animal is more circular, its velocity is smaller for the same value of the chemotactic parameter (*SI Appendix*, Fig. S5).

An indirect way to test these predictions experimentally is to monitor the motion of the animal at different temperatures of the water. Thermorheological experiments (36) using laser beams to heat a section of a microchannel, while measuring the instantaneous deformations of a single living breast epithelial cell, demonstrate that heat softens the cellular instantaneous rearrangements of the cytoskeleton. The long-term response or adaptation, which has to do with the changes in viscosity of the intracellular medium, was also investigated by performing experiments at various temperatures of the water. Both experiments imply that the mechanical response of the cell stiffens in cold water.

We have performed experiments studying the shape index of animals moving in water at different temperatures. The shape index is the ratio between the area of the animal and the area of a circle with the same perimeter.

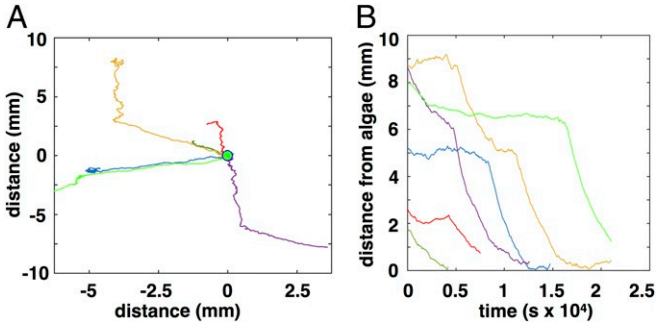

Fig. 3. (*A*) Trajectories obtained with simulations of *Trichoplax* in the presence of a focal food source. (*B*) Distance from the centroid of the animal to the food source for the tracks shown in *A*. The colors of the curves match the ones for the trajectories in *A*. Compare with the experimental results shown in Fig. 2.

An example of these experiments is shown in Fig. 5, where the shape index (squares) is plotted against the velocity at three different temperatures, and the time between consecutive measurements is 6 s. It is seen that our prediction is validated qualitatively. In the same figure, we show the results from model calculations (stars) by varying the Vicsek radius (*SI Appendix*, section C).

To validate the mechanisms proposed in the model and to compare quantitatively the trajectories of *Trichoplax* with the theoretical ones, we analyzed the distributions of step sizes obtained from experimental data and from simulations.

Chemotactic trajectories have been analyzed statistically, and the probability distributions of steps sizes have been adjusted to a general gamma function, which encompasses a whole family of statistical distributions. The probability density function is then,

$$f(x;\alpha,\beta)=\frac{\beta^{\alpha}x^{\alpha-1}e^{-\beta x}}{\Gamma(\alpha)}, \qquad [5]$$

where α and β are the shape and rate parameters characterizing the distribution, and $\Gamma(\alpha)$ is a complete gamma function.

We have analyzed the chemotactic theoretical trajectories in the same way and found that the parameters that best fit the curves are the same for both the experimental and theoretical distributions, indicating not only that step sizes generated by the theoretical model are similar on average to the experimental data, but the probability of observing steps of a specific size (their statistical distributions) are the same. In our case, 80% of the steps are small (smaller than the normalized distance ~ 1.6, equivalent to ~ 40 μm traversed in 10 s), only 5% of the steps are big (greater than 2.3 times the normalized distance, equivalent to steps between 73.9 and 151.9 μm traversed in 10 s), and this happens in both the observed data and our calculation. This quantitatively validates the hypotheses used in the theoretical model. Higher values of A_f correspond to more skewed distributions (smaller α).

In Fig. 6, we show a comparison between the empirical distributions of 10 experimental and theoretical chemotactic tracks ($N=560$). These were fitted using the same values of $\alpha=1.8$ and $\beta=0.50$, for both sets. The fitting is not shown because the curve overlaps perfectly with the empirical data.

We made another calculation with a higher number of cells (N = 5,000) to determine whether the probability distributions vary with the size of the system. We found that the adjustment of the former data, including the new big calculation, gave $\alpha=1.92$ and $\beta=0.52$, still within the 99% confidence interval for $\alpha=1.8$. Therefore, this demonstrates that the fitted curve in Fig. 6 does not change appreciably with N.

These comparisons allow us to conclude that the model closely reproduces the way in which *Trichoplax* moves toward food. The chemotactic mechanism directs it to food, but the random movements of individual ciliated cells and the fact that the cells are only partially synchronized by their interactions with other cells deviates the animal from its target. Its trajectory is not persistently directed toward the target but instead meanders, as is typical of cells and organisms that use stochastic mechanisms for chemotaxis.

Furthermore, the sensitivity analysis in *SI Appendix*, section C of the step size and the shape index allow determination of the value of elastic quantities used in the model with enough precision to be able to predict changes of behavior in future experiments.

Discussion

We show that *Trichoplax* moves preferentially up a chemoattractant gradient emanating from algae and develop a physical model based on known properties of its cells that explains this directed movement. In our model, directed movement arises from the collective motion of individual ciliated cells, each postulated to sense and respond to the chemoattractant. The movements of the cells are constrained by their junctions with neighboring cells and by elastic forces arising from other cells with which they are linked directly and via intervening cells. These constraints compel the cells to move as a cohesive group but allow local deviations in bearing that are manifest in the fluid-like movements of cells in the interior of the animal and by variations in its body outline. The movements of the model animal appear to be those of an intelligent being searching for and finding food but are the result of a few rules that obey the most elementary physics.

Many eukaryotic cells, including ciliated cells, exhibit chemotaxis (21, 30, 37–39). Information about the cellular mechanisms used for chemotaxis of ciliated cells comes primarily from studies of cells that swim. Ciliated microorganisms swim forward along helical trajectories interrupted by intermittent turns. Directional

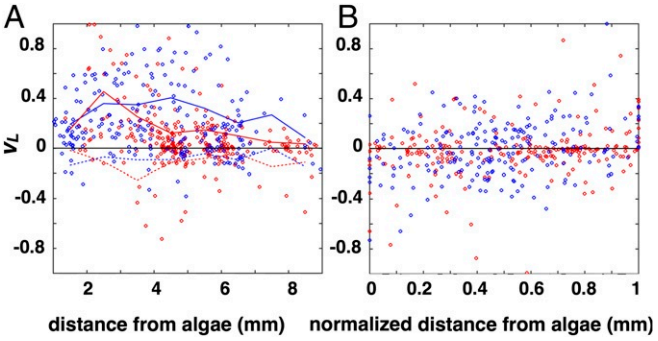

Fig. 4. (*A*) Scatter plot of the velocity component toward the food (v_L) as a function of the distance from the food source $\delta=|R_{cf}|$ for eight animals chemotaxing near the source. The velocity v_L was normalized to the maximum value of the whole set of experimental and numerical data. The red circles are the experimental measurements, and the blue ones the theoretical results. The blue and red continuous lines are the averaged positive velocities, and the dashed lines are the averaged negative velocities. The averages were taken in eight intervals of distance of length 1 mm. Observe that the positive velocities are much more abundant than the negative values, and that the averages of the theoretical and experimental data are very similar. (*B*) Same as *A* when the animals are in the distant range (from 6 to 18 mm). The distance in this case was normalized in the following way: $\delta_{(n)}=(\max(\delta)-\delta)/(\max(\delta)-\min(d))$; so both $|v_L|$ and δ are in the (0,1) interval. This is necessary because the distance range in each case varies wildly and comparison is difficult. This fact is not important, since the average value for both the blue and red circles is zero, and there is no particular trend.

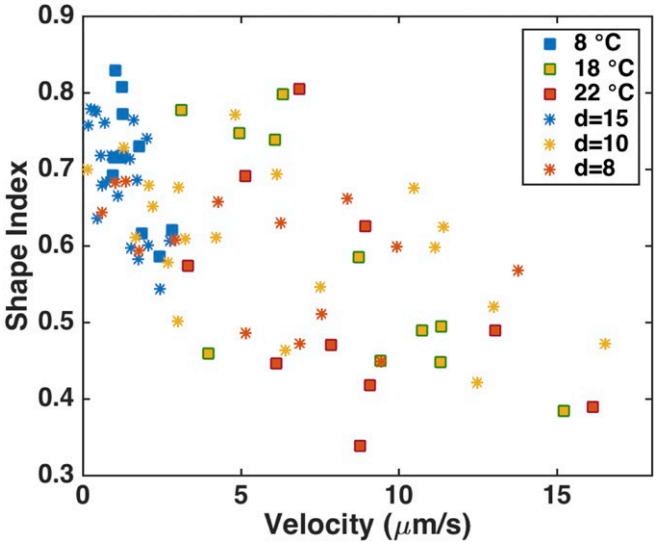

Fig. 5. The shape index of the animal as a function of the velocity at three different temperatures of the water (squares). Shape index as a function of the velocity using the three values for the Vicsek radius indicated in the legend in units of the minimum distance between cilia (stars).

motion in a chemotactic gradient depends on mechanisms to modulate ciliary beating as a function of the strength of the stimulus. Small ciliated cells typically use a stochastic navigation strategy, such as modulating the frequency of turns. Some larger cells, such as sperm, are able to adjust their helical paths so as to steer more persistently up the gradient (37, 38, 40, 41).

Our model assumes that the ciliated cells sense and respond to the chemoattractant gradient but does not depend on any particular chemotactic mechanism. In fact our model, as it is, predicts that in the absence of any chemotactic signal, the animal acquires a coherent motion, but it is not directed to a particular target (Movie S7). As a result, the center of mass moves randomly in a diffusive way, just like the real animal when it is far from algae or in an isotropic environment (42). However, the real animals also engage in additional behaviors not manifested by our model animal. For example, they occasionally pause even when no food is present. These spontaneous pauses are similar in duration to pauses that occur during feeding or in response to exogenous peptide (19), so we suspect that they are elicited by peptide secreted from gland cells, but why secretion might occur in the apparent absence of any sensory stimulus remains unknown. In addition, the animals sometimes stop migrating and rotate in place. Our model can be expanded to predict rotation under circumstances of enhanced traction of cilia around the rim and preferential beating in the tangential direction. We do not include these calculations in the present work because it remains to be seen what mechanisms exist in *Trichoplax* for regulating traction or beat direction of cilia.

Multicellularity has evolved multiple times in eukaryotes. Well-known examples are the volvocine algae, organisms that exist in both solitary and colonial forms. Their cells are biflagellate, and, in solitary cells, the flagella beat in a breast-stroke like motion to propel the cell forward. Colonies are spheroid with the cells arranged such that the effective strokes of the flagella push the colony in the same direction (43). Hydrodynamic coupling causes the flagella to beat in metachronous waves (44). The uniform beat direction and metachrony of the flagella of colonial volvocine algae contrasts with asynchronous and variable beat directions of cilia in *Trichoplax*.

Choanoflagellates also exist in solitary and colonial forms and are particularly relevant with regard to the evolution of Metazoa because they are the closest sister group (45). Choanoflagellates have a single cilium surrounded by a collar of microvilli, somewhat similar to the ciliated epithelial cells of *Trichoplax*. The choanoflagellate cilium beats in an undulatory waveform drawing water currents into the microvillar collar, to capture bacteria, and propelling swimming (46). The colonial forms consist of clusters of fewer than 50 cells, each with its cilium directed outward. The cilia of cells in colonies beat asynchronously and propel the animal along meandering trajectories typical of random walkers (47). Colonial organisms that use this form of locomotion have been referred to as aggregate random walkers, an apt description of *Trichoplax*. Directed movement of both unicellular and colonial choanoflagellates in an oxygen gradient, aerotaxis, has been reported (31). Analysis of the navigation strategy showed that it is of the stochastic type and achieved by modulating the angle of turns with respect to the direction of the gradient. The trajectories of the colonies are highly erratic and do not exhibit the striking persistence in the direction up the gradient that is evident in both *Trichoplax* and our model animal. This persistent movement is a property that emerges from the combined interactions between cells choreographed and mediated by the cell junctions and the fiber cell connections. This produces the effect that correlations are extended over larger distances, so the correlation length due to elastic interactions increases.

The mechanism we propose for directed ciliary gliding in *Trichoplax* probably could not work in animals much larger than a few millimeters in diameter, because of the fact that the medium-range interactions needed to produce a swarm behavior have an upper limit imposed by the actual value of the elastic moduli of the materials being bonded and by the mass that needs to be moved. As we enlarge the animal, the number of cilia scales with the surface while the mass scales with the volume. Therefore, there is a point at which there is not sufficient propulsion to move the mass.

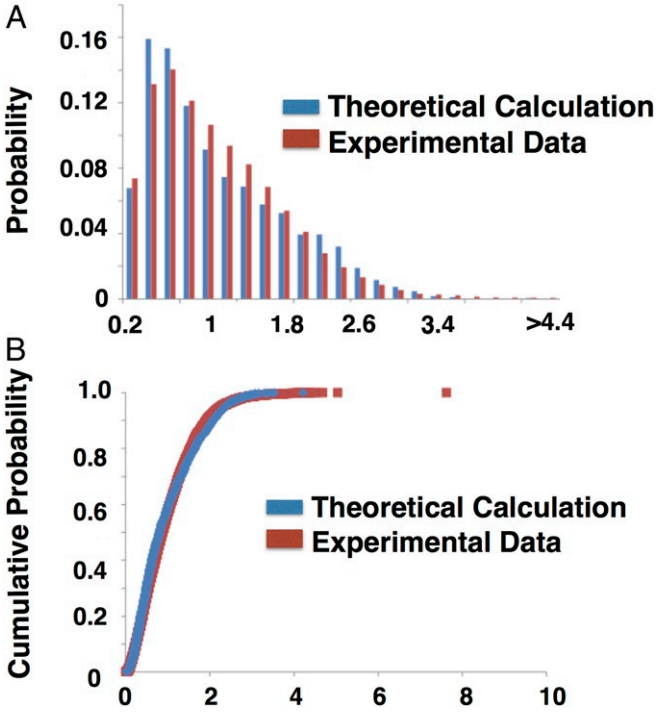

Fig. 6. Comparison of the probability distributions of steps for 10 experimental and 10 theoretical trajectories. (*A*) Probability histogram. (*B*) Cumulative probability comparison using the same parameters.

Ciliary gliding is used by many small invertebrates such as the larvae of some Cnidaria, as well as some larger bilaterians such as Platyhelminthes (flatworms) and some molluscs (48, 49). In all examples that we are aware of, the organism has a well-defined anterior–posterior axis, and the cilia beat in a uniform direction with respect to that axis. The animal uses muscles and a nervous system to control the direction of gliding. Evolution of large gliding animals probably was not possible before the origin of neurons and muscles.

Trichoplax has been considered a representative of an animal at an intermediate stage in the evolutionary trajectory from a choanoflagellate-like ancestor to complex metazoans with muscles and nervous and internal digestive systems (50, 51). Recent work (8, 19, 52–55) has emphasized the many similarities between *Trichoplax* and complex metazoans, such as possession of neurosecretory cells and cells that secrete digestive enzymes, intracellular communication by peptidergic signaling, and the orderly arrangement of cells of ventral epithelium into a gut-like tissue dedicated to feeding. Our present work calls attention to a way in which it could more closely resemble a colonial ancestor composed of self-propelled cells that behave independently and work together only because they are coupled and constrained by their connections to each other. While this mechanism for directed movement toward food appears primitive, it evidently has enabled the Placozoa to survive for a very long time. Molecular clock analyses place the origin of the phylum Placozoa in the Cryogenian, but there is no fossil evidence that could reveal when placozoans acquired their present body plan. Their lifestyle and mode of feeding appear well-suited to survival during Precambrian times, when the sea bottom was covered by microbial mats, the food that sustains extant placozoans, so it seems plausible that they already had acquired this lifestyle by that time.

Materials and Methods

T. adhaerens, a gift from Leo Buss, Yale University, New Haven, CT, were maintained in culture dishes with *Rhodomonas salina* algae as a food source as described previously [Smith et al. (18)]. Cultures of *R. salina* were maintained in artificial seawater (ASW) (Instant Ocean) with 1% Micro Algae Grow (Florida Aqua Farms). For use in chemotaxis assays, algae were concentrated by centrifugation and suspended in low melting-point agarose ($\sim 10^5$ cells/10 μL). Solidified agar containing algae was sliced into disks $\sim$3 mm in diameter. A disk was placed in the center of a 50-mm glass Petri dish, and then the dish was flooded with 4 mL of agar (1.7% in ASW) at 37–40 °C. After the agar cooled and solidified, 10 mL of ASW was added. The dish was kept at room temperature for 1–2 hours and filled with 10 mL of fresh ASW before use. Thirteen to 20 *Trichoplax* were placed in the dish at varying distances from the algae pellet. The dish was placed on a precision light box (Northern Light Imaging) set to provide low-intensity illumination. The temperature was maintained at 18°C with a temperature controller. Time-lapse recordings (six frames per minute) were captured with a Canon EOS 5D Mark III 22.3 MP Digital Camera equipped with Canon MP-E 6 5 mm f/2.8 1–5× Macro Photo lens. EOS Utility 2.13.40.2 software was used to control the camera and collect images. The behavior of animals was examined in time-lapse movies from seven experiments lasting 14–28 h. We selected for analysis five experiments in which most of the animals remained separate from each other and excluded two in which many of them clustered together, intermittently pausing and moving in coordination, a type of behavior described previously (19). Volocity Image Analysis software (PerkinElmer) was used to track nine animals that migrated onto the algae pellet and nine that remained far from the algae. Animals that did not contact other animals were selected for analysis because the program could not accurately track animals contacting other animals. Tracks terminated when the outline of the animal fused with the outline of the algae pellet. Figures and movies were constructed from image sequences resampled to two frames per minute. The rate of diffusion of low-molecular-weight substances within 1.7% agar was estimated by observing diffusion of fluorescent dye (CF 633; Biotium) embedded in agar. Fluorescence images were captured with a 5× 0.25 NA objective on a LSM10 confocal microscope (Carl Zeiss Microscopy).

Statistical analysis of probability distributions was made using the software SAS. The parameter α we found was within the 99% confidence interval of (1.85, 1.99) for the experimental data, (1.69, 1.96) for the simulations with $N = 560$, and (1.88, 2.2) for N = 5,000. The parameter β was within the 99% confidence interval of (0.49, 0.54) for the experimental data, (0.50, 0.59) for the simulations with $N = 560$, and (0.45, 0.54) for N = 5,000. The source code for the model is available upon request.

ACKNOWLEDGMENTS. We thank Tatiana Mayorova and John Chludzinski for assistance with time-lapse imaging and Joshua Zimmerberg, Shahid Khan, and Philip Maini for helpful comments on the manuscript. R.A.B. is grateful for a sabbatical grant from Direccion General de Asuntos del Personal Academico, Programa de Apoyos para la Superacion del Personal Academico de la Universidad Nacional Autonoma de Mexico, and acknowledges financial support from Conacyt, through Project 283279. This work was supported by the Intramural Research Program of the NIH, National Institute of Neurological Disorders and Stroke.

1. Moroz LL, et al. (2014) The ctenophore genome and the evolutionary origins of neural systems. *Nature* 510:109–114.
2. Ryan JF, et al. (2013) The genome of the ctenophore Mnemiopsis leidyi and its implications for cell type evolution. *Science* 342:1242592.
3. Simion P, et al. (2017) A large and consistent phylogenomic dataset supports sponges as the sister group to all other animals. *Curr Biol* 27:958–967.
4. Whelan NV, et al. (2017) Ctenophore relationships and their placement as the sister group to all other animals. *Nat Ecol Evol* 1:1737–1746.
5. Whelan NV, Kocot KM, Moroz LL, Halanych KM (2015) Error, signal, and the placement of Ctenophora sister to all other animals. *Proc Natl Acad Sci USA* 112:5773–5778.
6. Leys SP, Riesgo A (2012) Epithelia, an evolutionary novelty of metazoans. *J Exp Zool B Mol Dev Evol* 318:438–447.
7. Smith CL, Reese TS (2016) Adherens junctions modulate diffusion between epithelial cells in *Trichoplax adhaerens*. *Biol Bull* 231:216–224.
8. Smith CL, et al. (2014) Novel cell types, neurosecretory cells, and body plan of the early-diverging metazoan it Trichoplax adhaerens. *Curr Biol* 24:1565–1572.
9. Gibbons IR (1961) The relationship between the fine structure and direction of beat in gill cilia of a lamellibranch mollusc. *J Biophys Biochem Cytol* 11:179–205.
10. Lindemann CB, Lesich KA (2010) Flagellar and ciliary beating: The proven and the possible. *J Cell Sci* 123:519–528.
11. Sleigh MA (1962) The movement of cilia and flagella. *The Biology of Cilia and Flagella*, International Series of Monographs on Pure and Applied Biology: Zoology (Pergamon, Oxford), Vol 12, pp 127–169.
12. Tamm SL, Tamm S (1981) Ciliary reversal without rotation of axonemal structures in ckenophone comb plates. *J Cell Biol* 89:495–509.
13. Green CR (1989) Cnidarian gap junctions: Structure, function and evolution. *Evolution of the First Nervous Systems* (Springer, Boston), pp 3–20.
14. Panchin Y (2005) Evolution of gap junction proteins–The pannexin alternative. *J Exp Biol* 208:1415–1419.
15. Srivastava M, et al. (2008) The *Trichoplax* genome and the nature of placozoans. *Nature* 454:955–960.
16. Grell KG, Ruthmann A (1991) Placozoa. *Microscopic Anatomy of Invertebrates*, eds Harrison FW, Westfall JA (Wiley-Liss, New York), pp 13–27.
17. Armon S, Bull MS, Aranda-Diaz AJ, Prakash M (2018) Ultrafast epithelial contractions provide insights into contraction speed limits and tissue integrity. *Proc Natl Acad Sci USA* 115:E10333–E10341.
18. Smith CL, Pivovarova N, Reese TS (2015) Coordinated feeding behavior in *Trichoplax*, an animal without synapses. *PLoS One* 10:e0136098.
19. Senatore A, Reese TS, Smith CL (2017) Neuropeptidergic integration of behavior in *Trichoplax adhaerens*, an animal without synapses. *J Exp Biol* 220:3381–3390.
20. Ruthmann A, Behrendt G, Wahl R (1986) The ventral epithelium of *Trichoplax adhaerens* (Placozoa): Cytoskeletal structures, cell contacts and endocytosis. *Zoomorphology* 106:115–122.
21. Perez-Miravete A, ed (1973) *Behaviour of Micro-organisms* (Springer, Boston).
22. Heyland A, Croll R, Goodall S, Kranyak J, Wyeth R (2014) *Trichoplax adhaerens*, an enigmatic basal metazoan with potential. *Methods Mol Biol* 1128:45–61.
23. Vicsek T, Czirók A, Ben-Jacob E, Cohen I, Shochet O (1995) Novel type of phase transition in a system of self-driven particles. *Phys Rev Lett* 75:1226–1229.
24. Jayaraman G, et al. (2012) Autonomous motility of active filaments due to spontaneous flow-symmetry breaking. *Phys Rev Lett* 109:158302.
25. Grossman D, Aranson IS, Jacob EB (2008) Emergence of agent swarm migration and vortex formation through inelastic collisions. *New J Phys* 10:023036.
26. Szabó B, et al. (2006) Phase transition in the collective migration of tissue cells: Experiment and model. *Phys Rev E* 74:061908.
27. Ferrante E, Target AE, Dorigo M, Huepe C (2013) Elasticity-based mechanism for the collective motion of self-propelled particles with springlike interactions: A model system for natural and artificial swarms. *Phys Rev Lett* 111:268302.
28. Henkes S, Fily Y, Marchetti MC (2011) Active jamming: Self-propelled soft particles at high density. *Phys Rev E* 84:040301.
29. Hatwalne Y, Ramaswamy S, Rao M, Simha RA (2004) Rheology of active-particle suspensions. *Phys Rev Lett* 92:118101.
30. Leick V, Hellung-Larsen P (1992) Chemosensory behaviour of Tetrahymena. *Bioessays* 14:61–66.

31. Kirkegaard JB, Bouillant A, Marron AO, Leptos KC, Goldstein RE (2016) Aerotaxis in the closest relatives of animals. *eLife* 5:1–16.
32. Barrio RA, et al. (2013) Cell pattern emerge from coupled chemical and physical fields with cell proliferation dynamics: The Arabidopsis thaliana root as a study system. *PLoS Comput Biol* 9:e1003026.
33. Orozco-Fuentes S, Barrio RA (2017) Modelling the dynamics of stem cells in colonic crypts, *Eur Phys J Spec Top* 226:353–363.
34. Fletcher AG, Osterfield M, Baker RE, Shvartsman SY (2014) Vertex models of epithelial morphogenesis. *Biophys J* 106:2291–2304.
35. Mirabet V, Das P, Boudaoud A, Hamant O (2011) The role of mechanical forces in plant morphogenesis. *Annu Rev Plant Biol* 62:365–385.
36. Kießling TR, Roland S, Käs JA, Fritsch AW (2013) Thermorheology of living cells—Impact of temperature variations on cell mechanics. *New J Phys* 15:045026.
37. Alvarez L (2017) The tailored sperm cell. *J Plant Res* 130:455–464.
38. Kaupp UB, Alvarez L (2016) Sperm as microswimmers–Navigation and sensing at the physical limit. *Eur Phys J Spec Top* 225:2119–2139.
39. Van Houten J (1978) Two mechanisms of chemotaxis in Paramecium. *J Comp Physiol* 127:167–174.
40. Friedrich BM, Julicher F (2007) Chemotaxis of sperm cells. *Proc Natl Acad Sci USA* 104:13256–13261.
41. Kaupp UB, Kashikar ND, Weyand I (2008) Mechanisms of sperm chemotaxis. *Annu Rev Physiol* 70:93–117.
42. Ueda T, Koya S, Maruyama YK (1999) Dynamic patterns in the locomotion and feeding behaviors by the placozoan *Trichoplax adhaerence*. *Biosystems* 54:65–70.
43. Ueki N, Matsunaga S, Inouye I, Hallmann A (2010) How 5000 independent rowers coordinate their strokes in order to row into the sunlight: Phototaxis in the multicellular green alga Volvox. *BMC Biol* 8:103.
44. Brumley DR, Polin M, Pedley TJ, Goldstein RE (2012) Hydrodynamic synchronization and metachronal waves on the surface of the colonial alga volvox carteri. *Phys Rev Lett* 109:268102.
45. King N, et al. (2008) The genome of the choanoflagellate Monosiga brevicollis and the origin of metazoans. *Nature* 451:783–788.
46. Dayel MJ, King N (2014) Prey capture and phagocytosis in the choanoflagellate salpingoeca rosetta. *PLoS One* 9:e95577.
47. Kirkegaard JB, Marron AO, Goldstein RE (2016) Motility of colonial choanoflagellates and the statistics of aggregate random walkers. *Phys Rev Lett* 116:038102.
48. Clark RB (1981) Locomotion and the phylogeny of the metazoa. *Bolletino Di Zool* 48:11–28.
49. Martin GG (1978) Ciliary gliding in lower invertebrates. *Zoomorphologie* 91:249–261.
50. Arendt D, Benito-Gutierrez E, Brunet T, Marlow H (2015) Gastric pouches and the mucociliary sole: Setting the stage for nervous system evolution. *Philos Trans R Soc Lond B Biol Sci* 370:20150286.
51. Syed T, Schierwater B (2002) Trichoplax adhaerens: Discovered as a missing link, forgotten as a Hydrozoan, re-discovered as a key to Metazoan evolution. *Vie Milieu* 52:177–187.
52. Liebeskind BJ, Hillis DM, Zakon HH, Hofmann HA (2015) Complex homology and the evolution of nervous systems. *Trends Ecol Evol* 31:127–135.
53. Moran Y, Barzilai MG, Liebeskind BJ, Zakon HH (2015) Evolution of voltage-gated ion channels at the emergence of Metazoa. *J Exp Biol* 218:515–525.
54. Senatore A, Raiss H, Le P (2016) Physiology and evolution of voltage-gated calcium channels in early diverging animal phyla: Cnidaria, Placozoa, Porifera and Ctenophora. *Front Physiol* 7:1–26.
55. Varoqueaux F, Fasshauer D (2017) Getting nervous: An evolutionary overhaul for communication. *Annu Rev Genet* 51:455–476.